nature COMMUNICATIONS

Supplementary Materials for

Short-Term Interaction between Silent and Devastating Earthquakes in Mexico

Authors: V. M. Cruz-Atienza*, J. Tago, C. Villafuerte, M. Wei,
R. Garza-Girón, L. A. Dominguez, V. Kostoglodov, T. Nishimura,
S. I. Franco, J. Real, M. A. Santoyo, Y. Ito and E. Kazachkina.

*Correspondence to: cruz@geofisica.unam.mx

This PDF file includes:

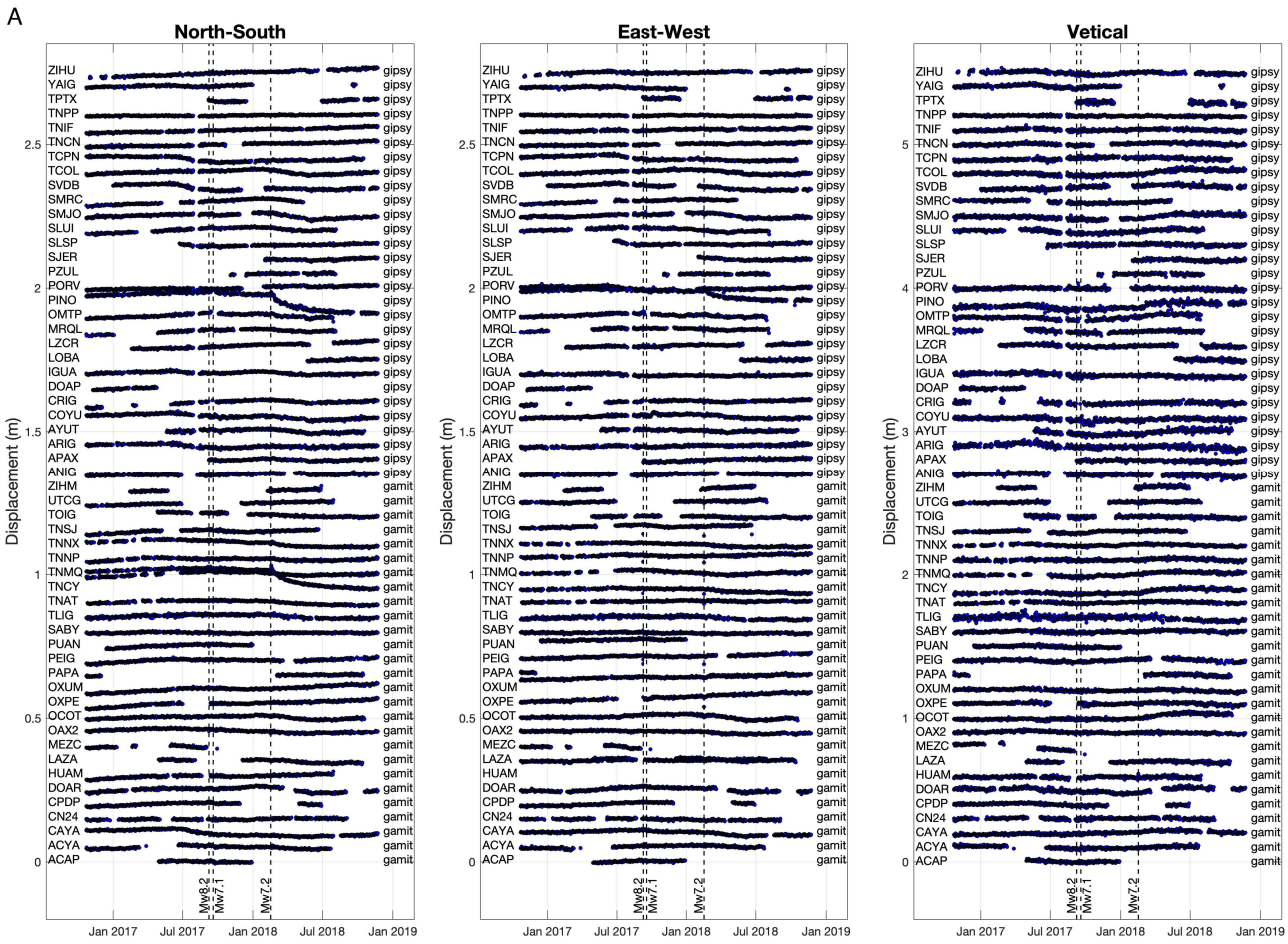

Fig. S1. Displacement GPS time series in 57 selected stations (A) from October 23 (2016) to November 22 (2018) and (B) from November 22 (2018) to October 8 (2019). To the right of each series is indicated the data processing method selected for the inversions. Vertical dashed lines indicate the occurrence of the three earthquakes of the sequence.

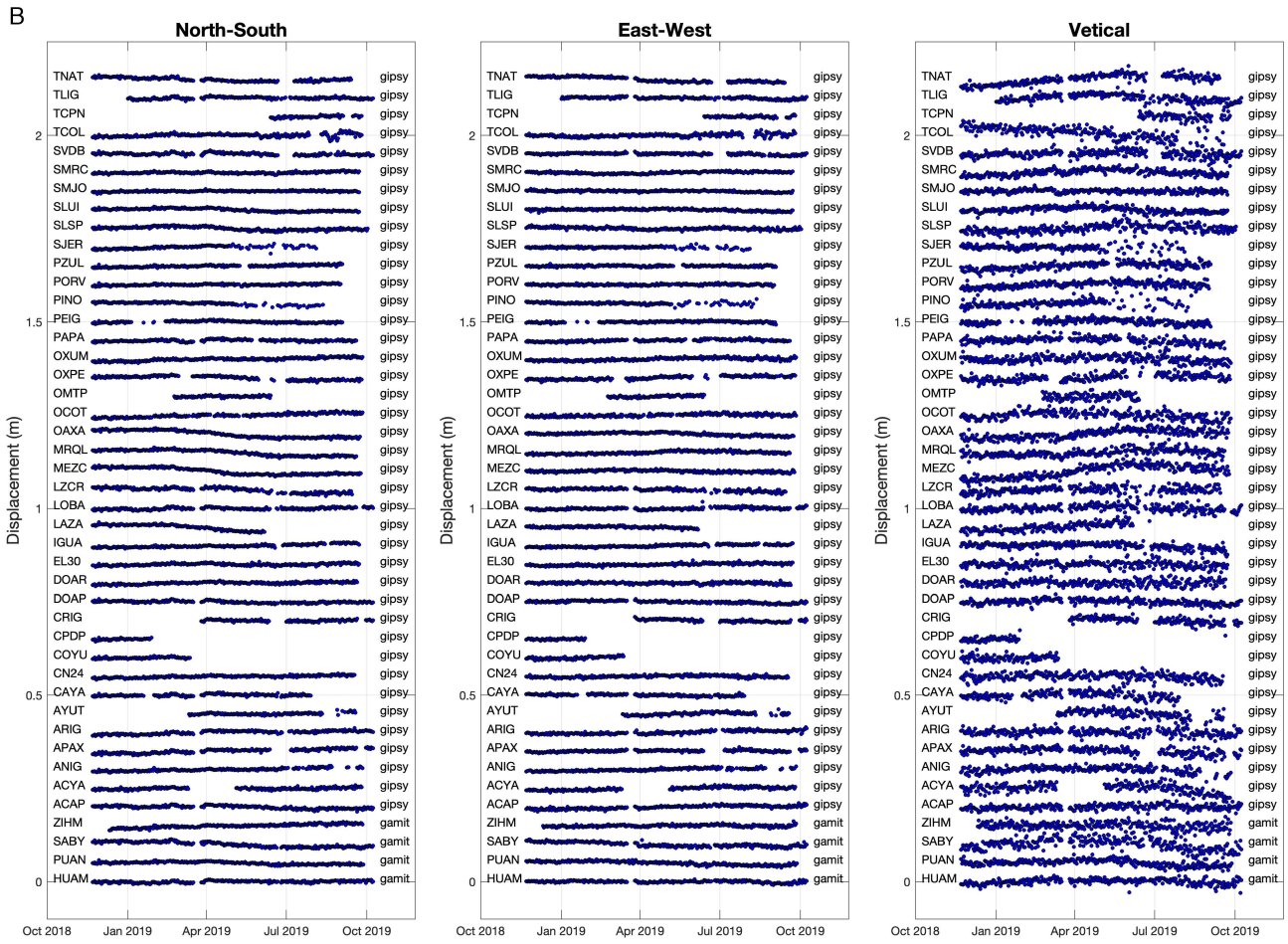

Fig. S1 (Continuation).

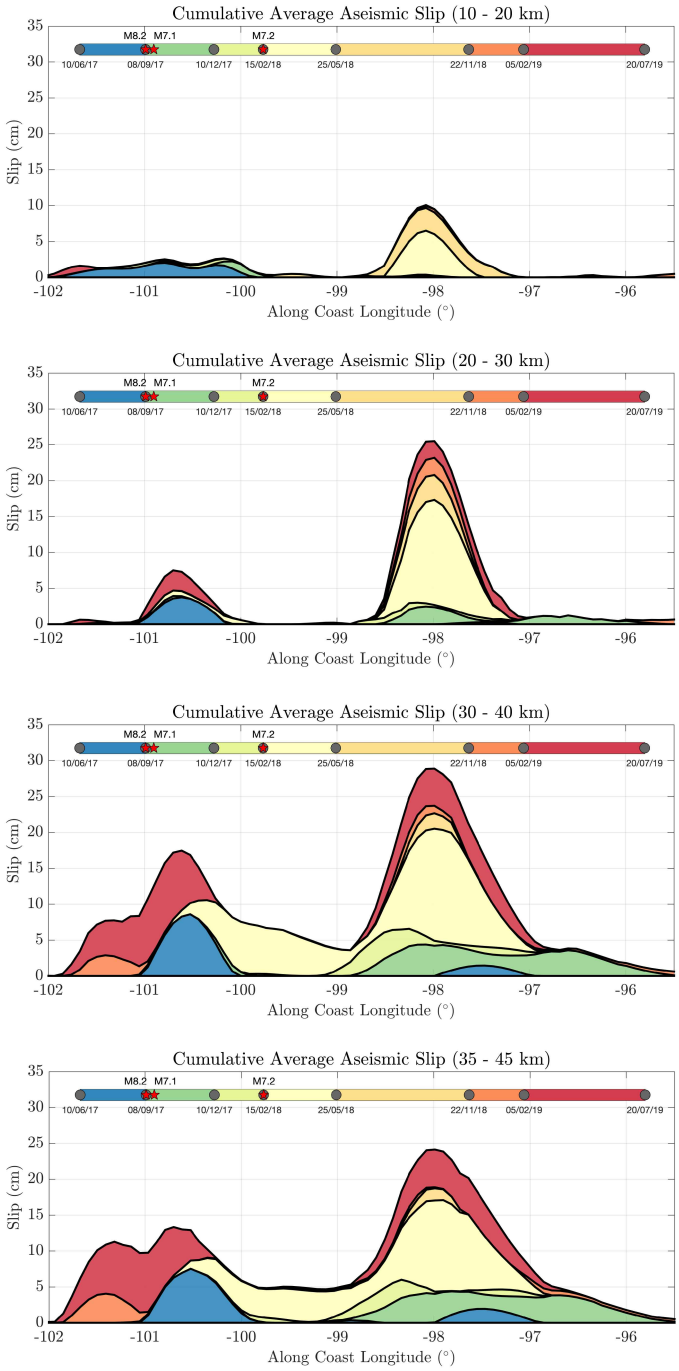

1

2 **Fig. S2.** Cumulative slow slip time history, averaged for different depth ranges (see panel titles),

3 from solutions shown in Fig. 2. Between 10 and 20 km depth (i.e. mainly offshore), only the 2017

Guerrero SSE and the Pinotepa earthquake post-seismic slip are significant, with maximum slip of 2.0 and 6.5 cm, respectively. The largest SSE activity concentrates between 20 and 45 km depth.

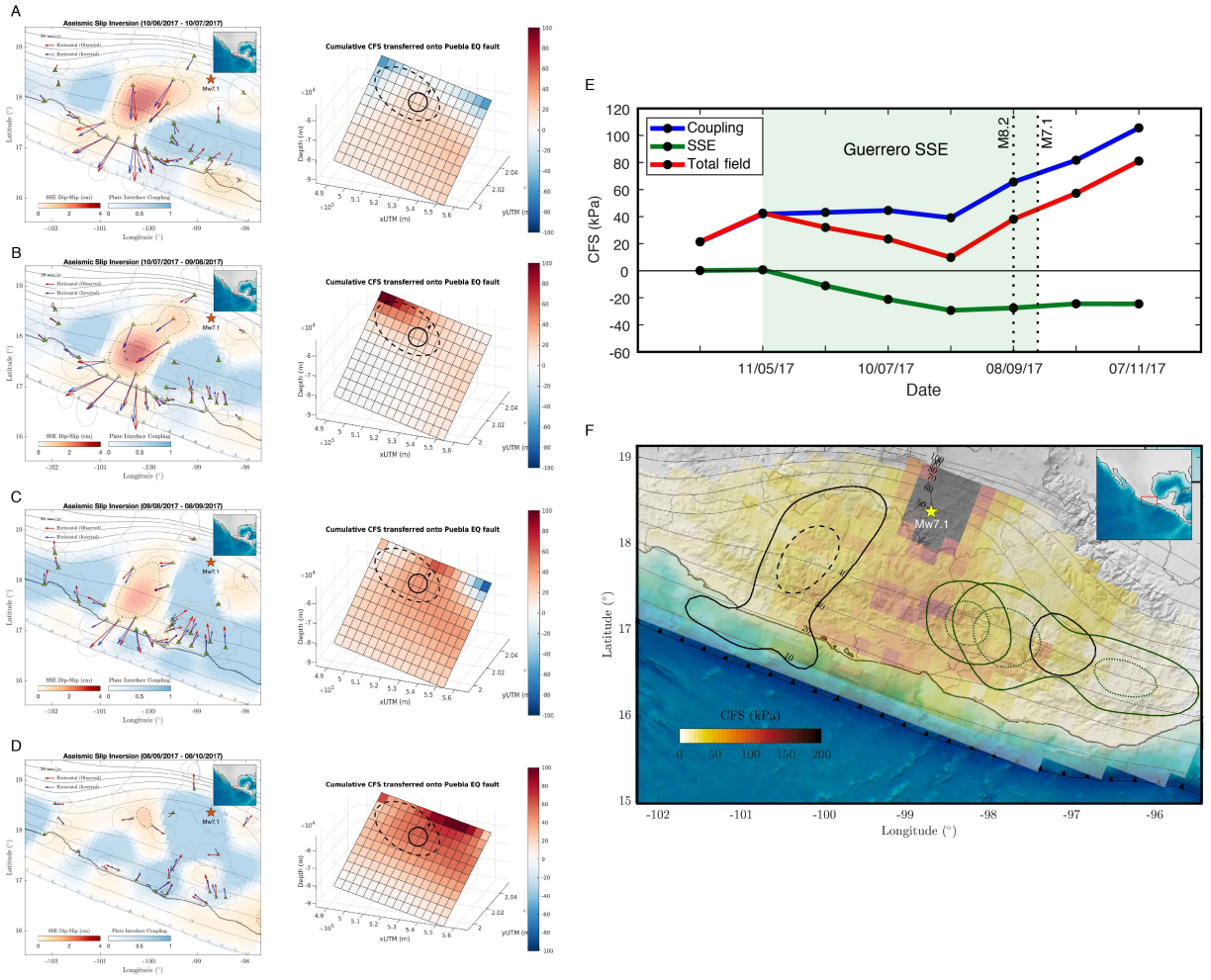

Fig. S3. (A-D) 30-day time windows aseismic slip inversions of the 2017 Guerrero SSE (left column) and the associated cumulative CFS over the intermediate-depth normal fault where the Mw7.1 Puebla-Morelos earthquake took place on September 19, 2017 (right column). Notice that the inverted time windows are shorter than those shown in Figs. 2 and S2. (E) CFS evolution within a 20 km radius from the Puebla-Morelos hypocenter. Notice the CFS sustained increment induced by the PIC in the later SSE stage. (F) CFS maximum values on the plate interface induced by the Puebla-Morelos earthquake. They were estimated with a 3D finite source simulation (see Fig. S9) similar to that performed for the Pinotepa earthquake (Fig. 5C) but using the finite-source solution determined by Mirwald et al. (*17*). Aseismic slip events right before the earthquake are shown with

black contours, while those occurred immediately after the earthquake are shown with green contours.

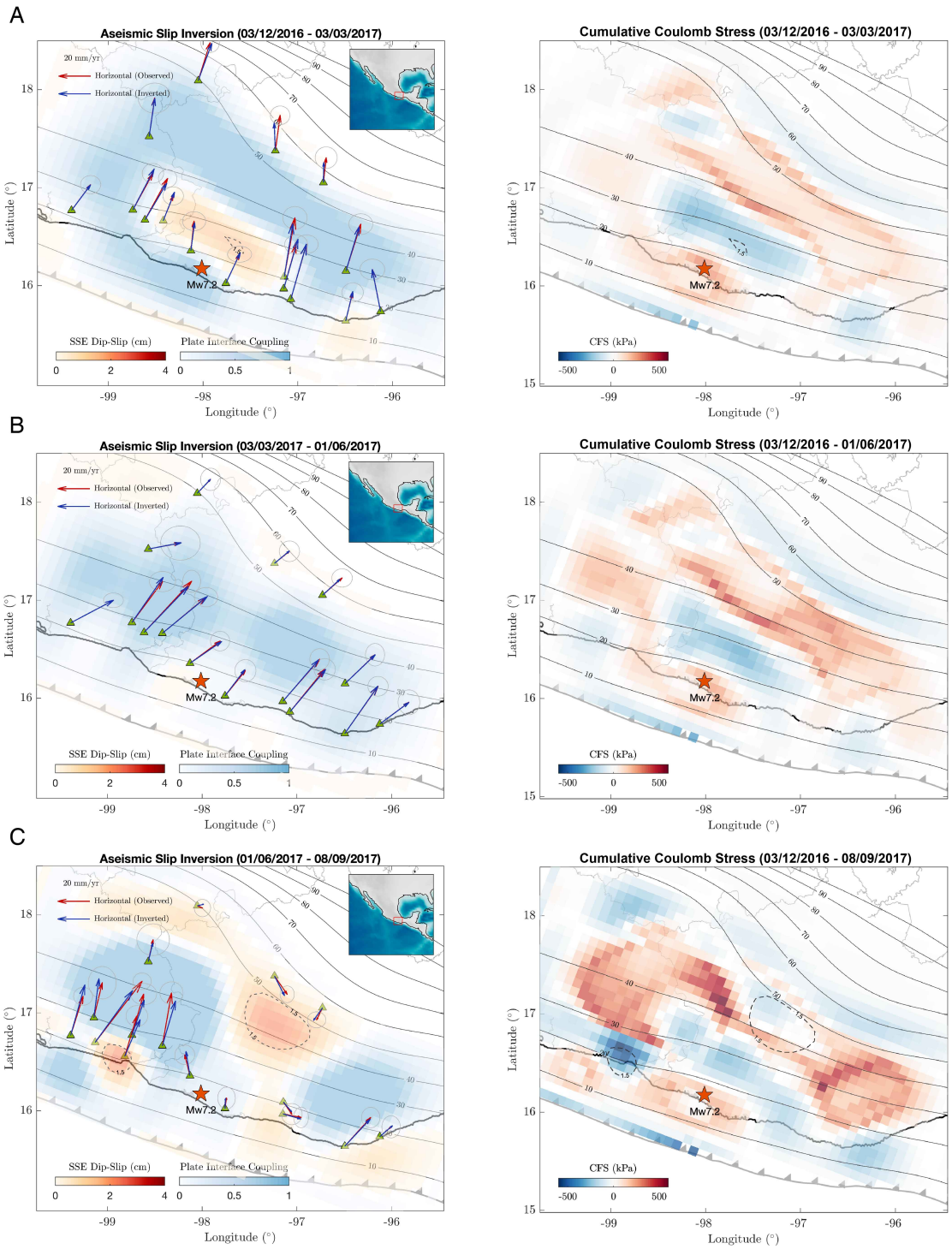

Fig. S4. Aseismic slip inversions preceding the Mw7.2 Pinotepa earthquake during the 2017 Oaxaca SSE (left column) and the associated cumulative CFS on the plate interface (right column). Dashed

contours in the right column show the aseismic slip contours of the associated time window. Notice that the inverted time windows are shorter than those shown in Fig. 2. Average CFSs from these higher time-resolution inversions are shown in Fig. 4B.

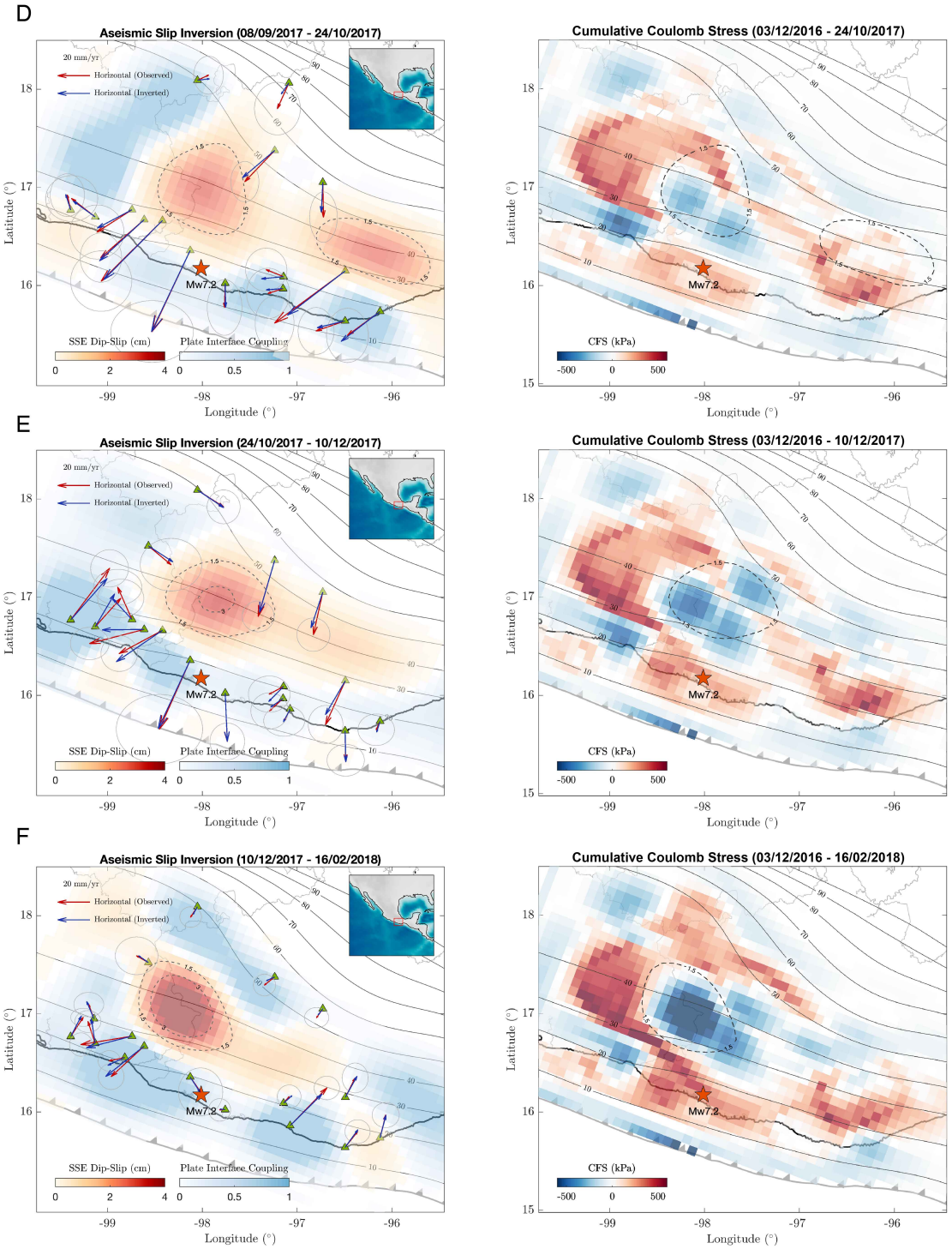

Fig. S4. (Continuation).

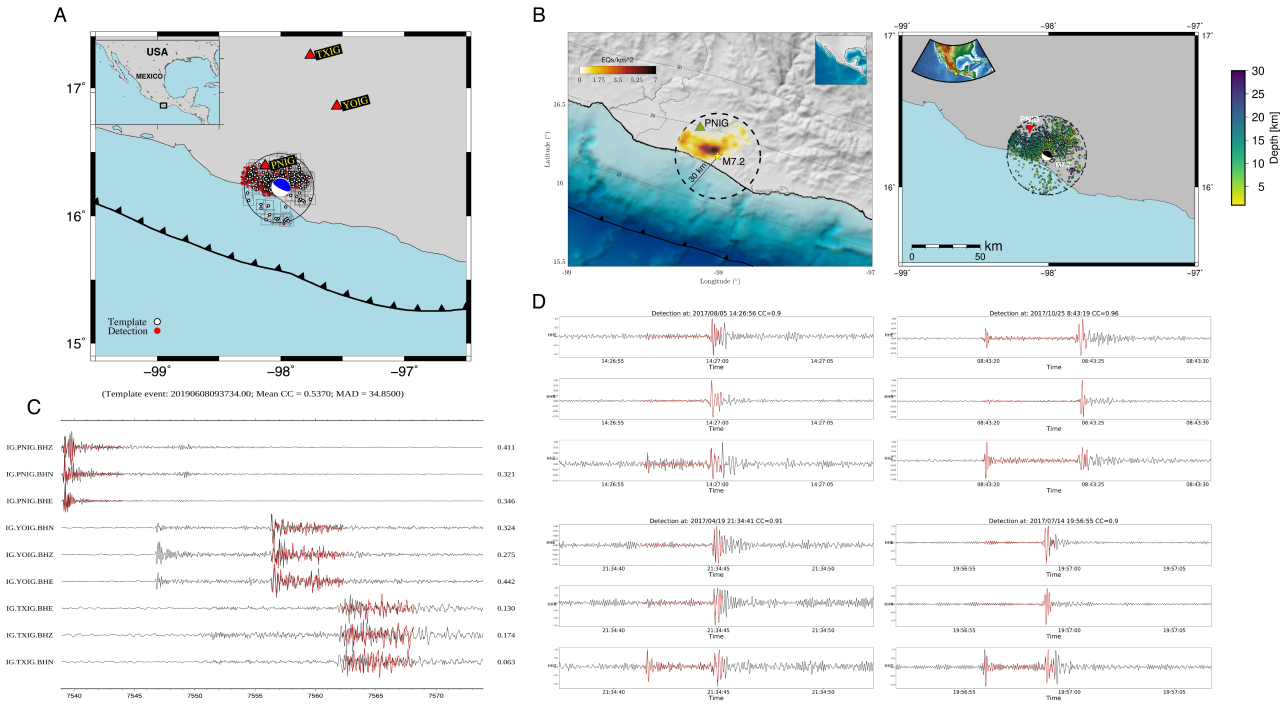

Fig. S5. Illustration of template matching results using two different methods. (A) Map of events detected by method 1 using three stations at a regional scale. (B) Density map for the template events used by method 2 (left) and their spatial distribution (right). (C) Example of a regional detection made at stations PNIG, YOIG and TXIG using method 1 for the direct S wave and its coda. (D) Examples of local detections made at station PNIG using method 2. The good fits of the templates that include both P and S direct waves and the coda of the P waves guarantee that detections come from the same hypocentral locations as the template events. See Figure 4 of the main text.

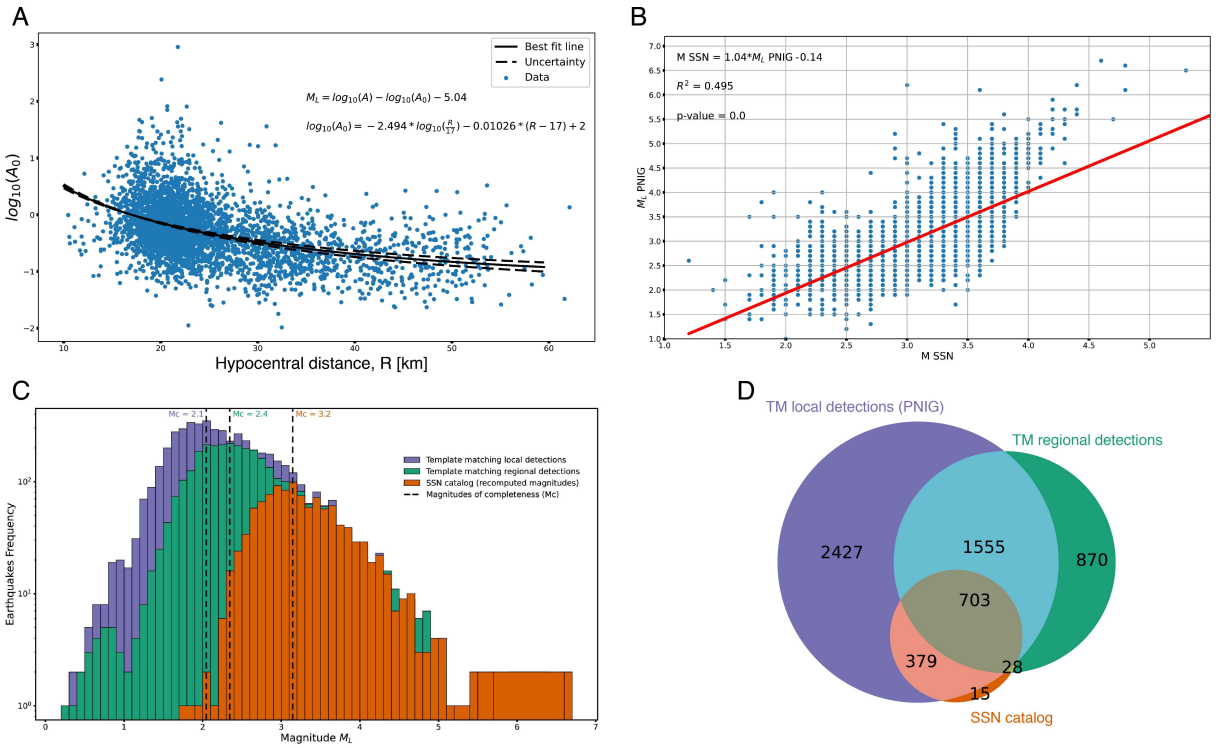

Fig. S6. Magnitude estimation for the template-matching (TM) newly detected earthquakes and final catalogs comparison. (A) Attenuation relationship calculated on the horizontal components (geometric mean) of PNIG and magnitude scale M_L. (B) Correlation between recomputed M_L magnitudes using the PNIG station and the magnitudes reported by the SSN. (C) Earthquake frequency distributions for the template matched catalogs using the closest station PNIG (blue), three stations of the regional network (green) and the catalog provided by the SSN (orange). (D) Venn diagram showing the relationship of the number of events of each catalog. The intersections are calculated by finding common events in time (events within 10 seconds of each other).

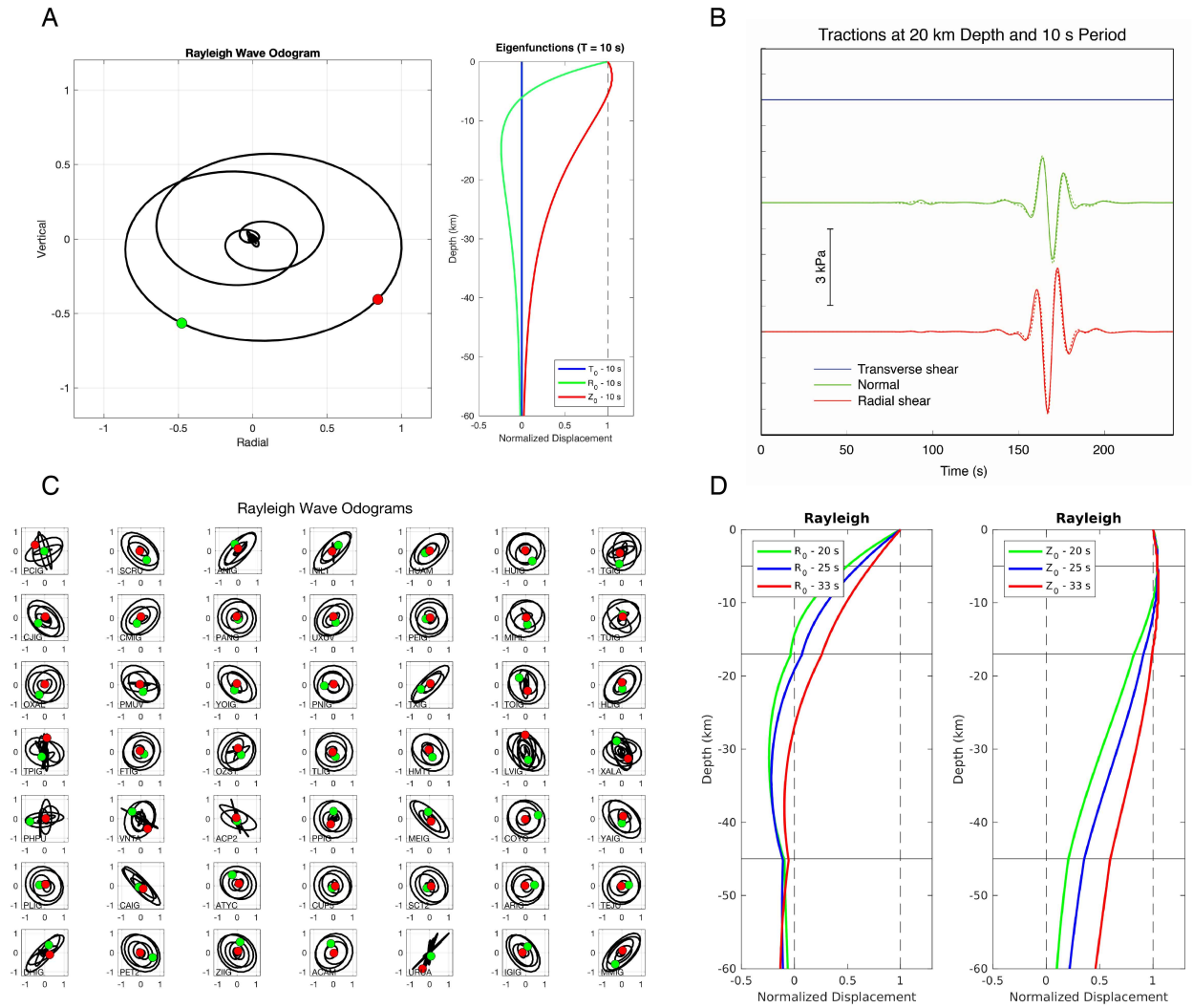

Fig. S7. Validation of the procedure to estimate dynamic perturbations on the plate interface from actual strong motion records. (A) Odogram of a Lamb pulse (i.e. of the wavefield produced by a vertical force applied at the free surface of a homogeneous halfspace) (left), and corresponding eigenfunctions for the Rayleigh wave fundamental mode at 10 s period (right). (B) Comparison at 20 km depth (horizontal plane) and 10 s period of the exact traction evolution (solid) and the estimated traction following the procedure described in Methods (dashed). (C) Odograms for the radial and vertical displacement components around 25 s period from actual records of the Mw8.2 Tehuantepec earthquake on 49 strong motion station (see Fig. S8). (D) Eigenfunctions of the

Rayleigh waves fundamental mode in a crustal 1D velocity model (*39*) used to estimate beneath each station the traction, CFS and dilation evolution on the 3D plate interface shown in Figs. 5A and S8.

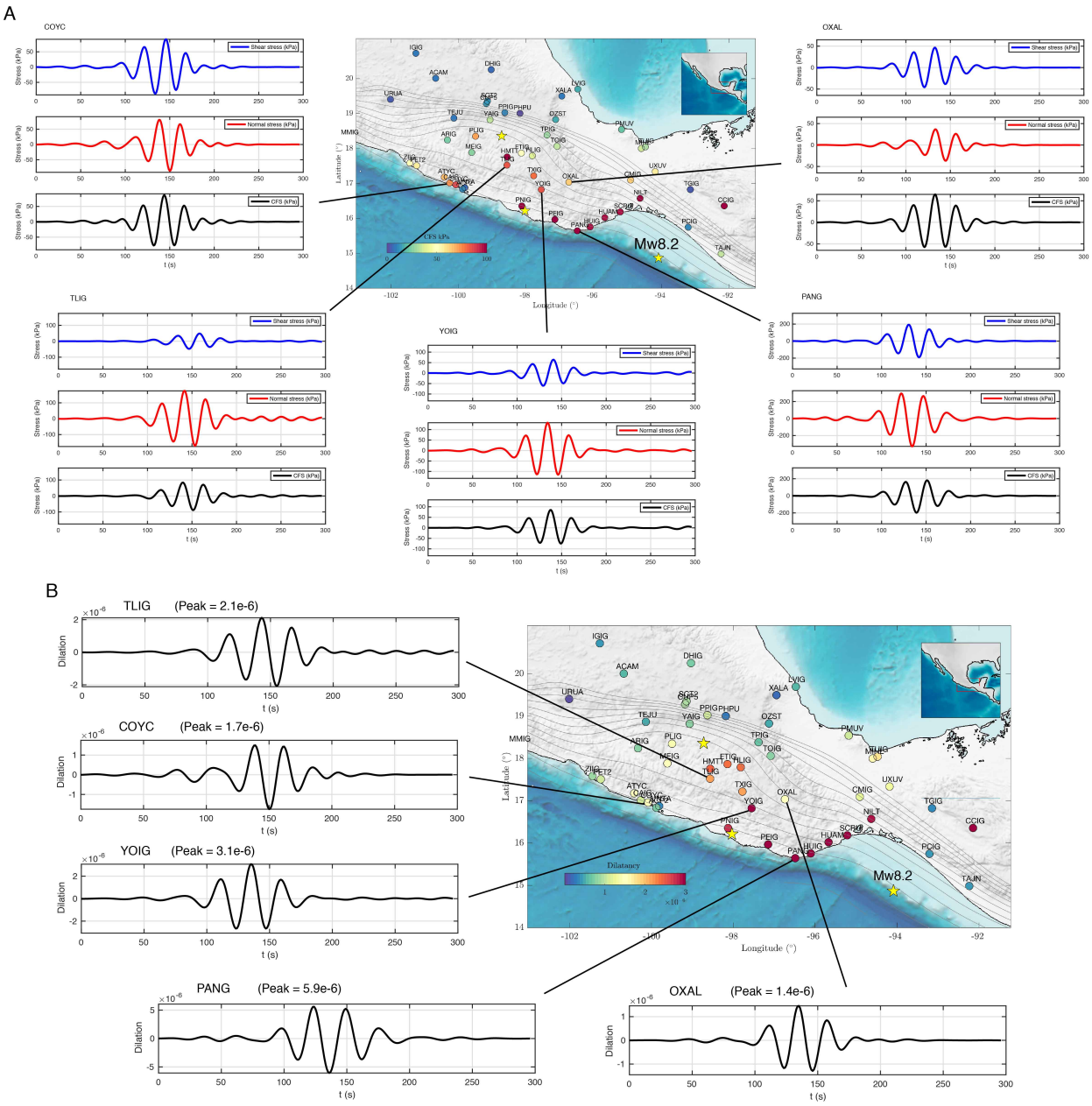

Fig. S8. 20 s period dynamic-stress (A) and dilation (B) perturbations over the 3D plate interface (gray contours) estimated from actual strong motion records of the Mw8.2 Tehuantepec earthquake below different seismic stations (circles). CFSs (computed in the plate-convergence slip direction) and dilations peak values are color-coded in each site. Values where there is no plate interface below correspond to 50 km depth over a horizontal surface.

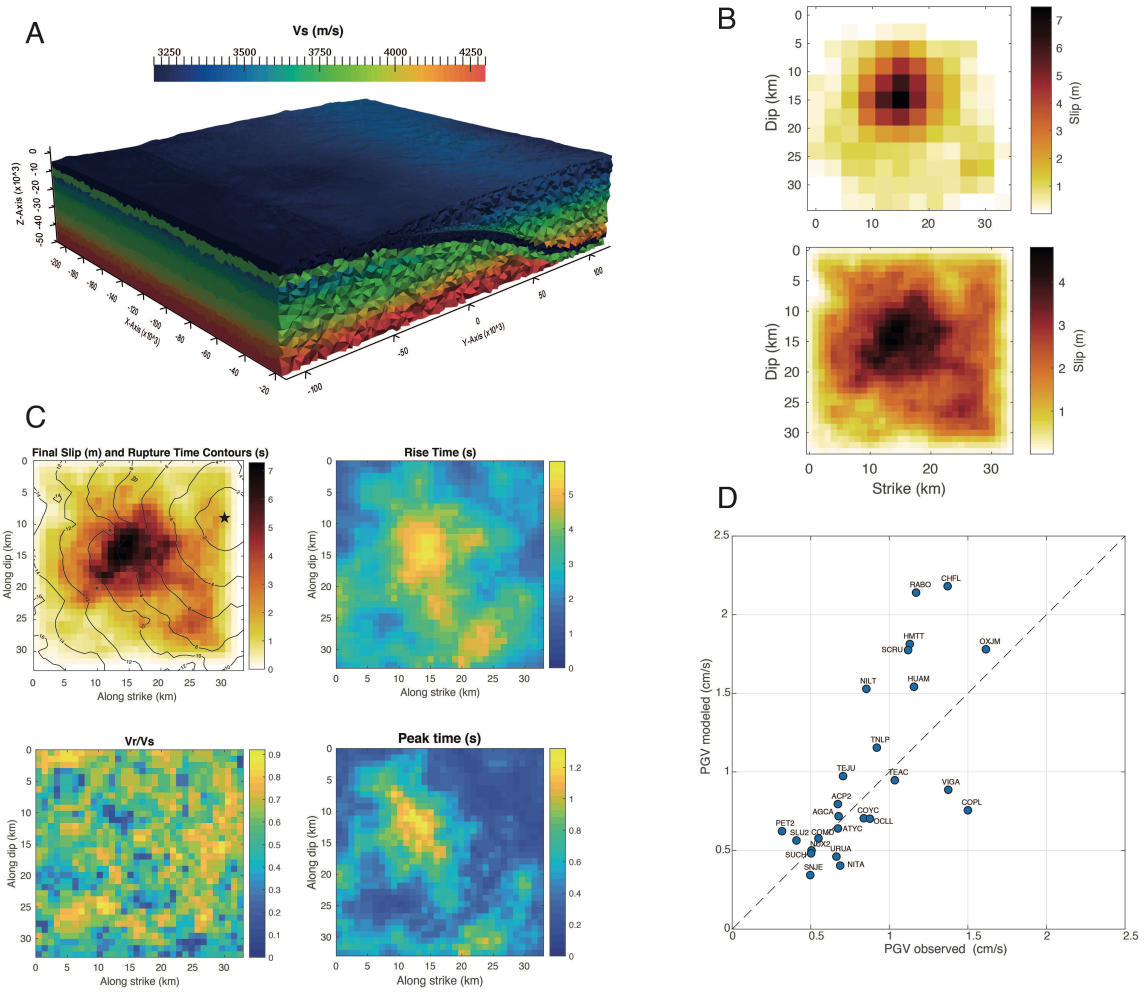

Fig. S9. 3D kinematic finite-source numerical simulation of the Mw7.2 Pinotepa earthquake. (A) Non-structured tetrahedral discretization of the Oaxaca subduction zone. (B) Initial USGS finite source inversion (up) and broad-band wavelength finite slip model (bottom). (C) Spatial distribution of the slip, the rise time, the rupture velocity and the peak time used to describe the kinematic rupture evolution. (D) Comparison between modeled and observed horizontal PGV for different hard-site strong motion stations (see Fig. S8 for site locations).

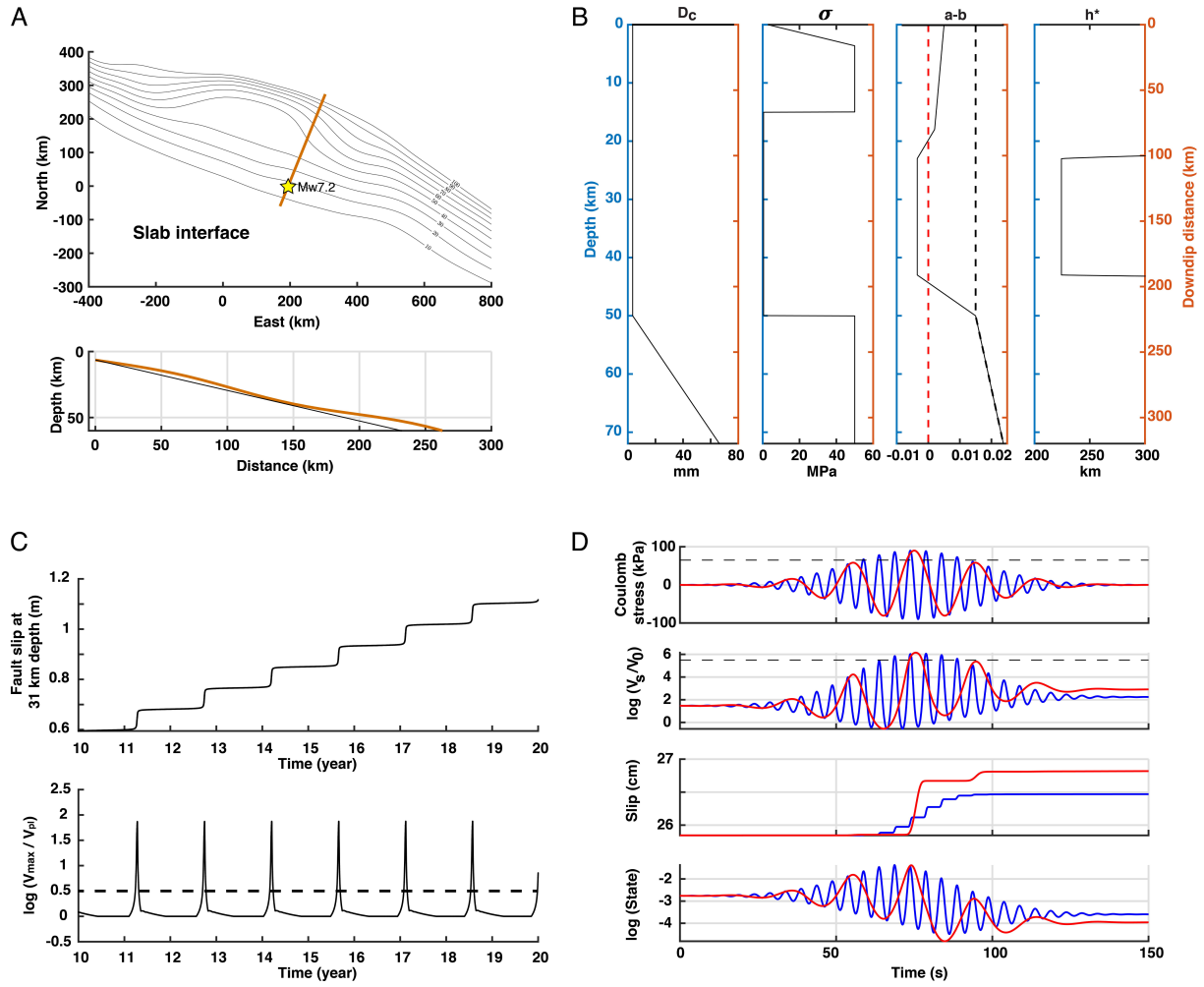

Fig. S10. (A) Top, slab geometry in the study area across the 2018 Mw7.2 Pinotepa earthquake epicenter. The orange solid line shows the profile of our 2D model over the 3D plate interface geometry. Bottom, the black solid line shows the planar fault model and the orange line shows the slab geometry. (B) Rate-and-state parameters used in our 2D reference model. Dc above 50 km is 3.5 mm. The effective normal stress in the low stress zone is 0.45 MPa. (C) Slip at 31 km depth and the maximum slip rate on the fault for the reference model. (D) Evolution of key model parameters with two different perturbations with different characteristic periods (5 s and 20 s periods) and same

60 kPa CFS peak values. Notice that longer period waves have significantly larger SSE triggering potential, i.e. ~40% larger final slip and much larger (effective) slip acceleration.